# Characterizing shallow subsurface using 3D seismic while drilling with a downhole pilot

Ali Aldawood[1], Mohammed Almarzoug[1], Ilya Silvestrov[1], and Andrey Bakulin[1]

https://doi.org/10.1190/tle41050304.1





## Abstract

Seismic while drilling (SWD) can provide high-resolution subsurface information and characterize near-surface geology. We present a case study of SWD analysis using a data set from a desert environment acquired over a complex overburden. The data were acquired with a system composed of wireless surface geophones as well as top-drive and downhole sensors. The drill-bit noise data were reprocessed using a specialized workflow with two essential elements. First, a downhole pilot from a near-bit sensor was used for deconvolution, which led to improved data quality, particularly in the shallow subsurface. Second, nonlinear beamforming leveraged the 3D carpet of geophones to enhance signal quality and enable picking 3D traveltimes. A simple workflow for building a 1D velocity model used 3D traveltimes from an offset of 180 to 500 m. We vertically projected and averaged all 3D traveltimes to obtain a robust checkshot profile for the section from 190 to 1855 m. For the shallow subsurface (0–800 m), we further applied an advanced workflow with 3D traveltime inversion that more accurately handled mid- and far-offset data using a ray-tracing engine. More than 100,000 offset traveltime picks were inverted for a 1D velocity model. The model closely ties with the geology of the near surface, namely the formation tops associated with major impedance and lithologic contrasts. Amplitude signatures of 3D SWD gathers also correlate with the velocity model and lithologic changes, showing weak energy associated with soft formations and higher-energy first-arrival waveforms associated with compacted formations. Finally, we used the data extracted from a 2D line to reconstruct a migrated image of the back-propagated drill-bit sources. Joint use of kinematic and dynamic signatures helps characterize markers associated with loss circulation zones and target layers.

## Introduction

Seismic while drilling (SWD) aims to illuminate the subsurface using the drill bit as a seismic source (Rector and Marion, 1991; Haldorsen et al., 1995; Miranda et al., 1996; Bertelli and di Cesare, 1999; Poletto and Miranda, 2004). The drill bit's vibrations are recorded by surface sensors, deconvolved using the recorded drill-bit signature, and processed to obtain reverse vertical seismic profiling data (Rector and Marion, 1991; Khaled et al., 1996; Miranda et al., 1996). Thus, SWD can provide real-time checkshot, locate bit on seismic, image ahead of the bit, etc. (Poletto and Miranda, 2004). This is all done without interfering with the drilling operation or incurring additional rig time. In addition, SWD assists various drilling decisions, especially those that require predicting accurate formation tops ahead of the bit with an uncertainty smaller than that allowed by surface seismic (Greenberg, 2008; Zhou et al., 2015).

While the business attractiveness of SWD is evident, the method poses several unique technical challenges. Weak drill-bit signals are challenging to record and process. In addition, high industrial noise makes data quality highly variable. Furthermore, a limited number of surface sensors typically placed along one or two orthogonal 2D lines further restricts data processing and velocity model building options. Al-Muhaidib et al. (2018) and Bakulin et al. (2020a) presented an SWD system called DrillCAM to try to overcome some of these challenges. In particular, the system utilizes novel wireless geophones to enable flexible 3D receiver geometry. With substantial variability of industrial surface noise and a changing complex near surface, 3D data increase the diversity of sensor placements and boost the chances to capture good-quality recordings. In addition, the diverse offsets and azimuths of a 3D layout provide a rich data set for focusing and traveltime inversion for subsurface velocity. Redundancy of the 3D data set makes it more immune to strong bursts of surface noise or data quality variations, which are quite typical for SWD data. For example, it was common to acquire checkshot velocity SWD surveys using a 2D line of surface sensors to identify the best possible receiver locations with a good signal-to-noise ratio (S/N) for velocity inversion. Such "lucky" receiver locations are hard to predict ahead of time. With advances in seismic wireless recording and transmission, it becomes feasible to use 3D sensor layouts to enable the modern data enhancement techniques required in a complex desert environment with extremely challenging seismic data quality (Bakulin et al., 2020a, 2020b). Three-dimensional data also enable more advanced workflows for 3D focusing and velocity model building. The DrillCAM system records two versions of a pilot signal — one with a top-drive sensor and another with the downhole near-bit tool.

This study focuses on characterizing the shallow subsurface from ground level to approximately 800 m using 3D SWD acquisition. Such characterization is especially critical in desert environments because this subsection is the most complex in terms of velocity variations. In particular, a complex near surface with highly contrasting layers may lead to severe challenges in seismic imaging (Bakulin and Silvestrov, 2021). Accurate shallow subsurface characterization holds the key to imaging and mapping low-relief structures (Bakulin et al., 2017). Unfortunately, the first-kilometer interval often represents a blind spot for conventional borehole geophysics, which struggles to produce reliable shallow measurements due to the imperfectly cemented multiple casing strings (Hardage, 2000; Bakulin et al., 2020a). When

[1]Saudi Aramco, EXPEC Advanced Research Center, Geophysics Technology, Dhahran, Saudi Arabia. E-mail: ali.dawood.18@aramco.com; mohammed.almarzoug.1@aramco.com; ilya.silvestrov@aramco.com; a_bakulin@yahoo.com.

logging from the surface is desired, it is possible to drill a pilot hole, conduct vertical seismic profiling (VSP), then enlarge and set casing and continue similar cycles for all shallow drilling runs. Such exceptions increase the risk and cost of the drilling operation. As a result, they are rarely done and only for special purposes.

Seismic uphole surveying that drills shallow holes to measure near-surface velocities is another practical method to characterize the immediate near surface. Upholes require a special crew and are limited to about 300 m depth. In contrast, the SWD survey continuously samples the subsurface starting from ground level without any interference with drilling. SWD does not require any modification to the drilling program and does not suffer from casing effects because it is performed while drilling an open hole. Shallow sections are characterized by large bit size and strong signals. Poletto et al. (2003) presented reverse SWD VSP data from a surface receiver at an offset of 1242 m away from the borehole, recording high-quality seismic wavefields illuminating reflectors at less than 1000 m deep. Rocca et al. (2005) showed a common-source gather (CSG) from a bit depth of about 469 m that has a relatively weak signal caused by seismic energy absorption in the shallow layers. Bakulin et al. (2020a) demonstrated a near-offset SWD checkshot up to a depth of 565 m with a top-drive pilot. This study uses dense single-sensor 3D data from the DrillCAM field trial (Bakulin et al., 2020a) and advanced processing with the downhole pilot recorded by the near-bit sensor. We demonstrate that a downhole pilot leads to a superior quality of 3D data in the shallow section. Three-dimensional geometry leads to 3D traveltime maps that are inverted for a high-resolution velocity model.

## SWD acquisition

Field data were acquired using about 2500 wireless receiver stations centered around the well (Figure 1a). Two different acquisition geometries were used: the first one for drilling 0–800 m and the second for 800 m and below. Figure 1 also identifies subsets of the 3D data set used for each of the three main tasks: velocity model building from shallow to deep (190–1855 m), source focusing and imaging (190–1856 m), and velocity model building for the shallow subsurface (190–800 m). Shallow subsurface characterization mainly benefits from the 3D central layout of the first geometry shown in Figure 1b. This patch contains about 2000 stations, each represented by a single geophone. An extensive drilling pad represents an active area with moving equipment and personnel. Despite the use of wireless stations (Bakulin et al., 2019), only a few locations around the center and edges were accessible for sensor placement (Figure 1b). As a result, near-offset traces needed to characterize shallow subsurface were primarily missed, while the remaining sensors at the rig site were often too noisy for useful checkshot surveys. Indeed, Bakulin et al. (2020a) utilized an offset of 475 m for SWD checkshot using a top-drive sensor pilot as a compromise, providing acceptable quality data from shallow to deep. However, the minimum pickable depth was only 565 m, while the upper portion of the data was too noisy.

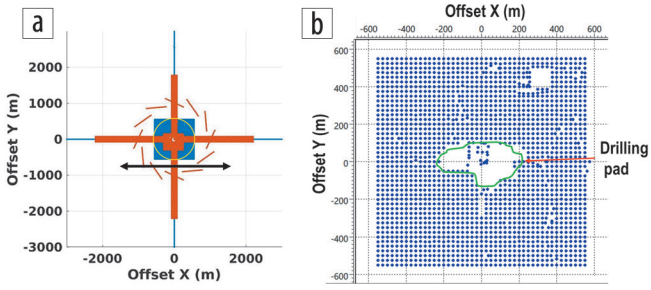


**Figure 1.** Receiver acquisition geometry used in the field trial with the drilling rig located at the origin: (a) geometry used for drilling 0–800 m is shown in blue, whereas geometry for drilling below 800 m is in orange. Each geometry uses 2500 single wireless geophones placed as dense 3D central patch and extended set of orthogonal 2D lines (east-west and north-south). (b) Zoom into central geophone patch used for shallow drilling (0–800 m) with the sampling interval of 25 m in both directions. Missing receivers are within active areas of the drilling pad. For velocity model building, simple and advanced workflows use 3D data inside yellow circle on (a) and full patch on (b), respectively. Source focusing exercise utilizes a subset of a 2D line shown by the black arrow (a).

In addition to surface geophones, the SWD system included a top-drive sensor and downhole vibration tool to measure the drill-bit signal required for deconvolution during processing (Bakulin et al., 2019, 2020a). Previous studies analyzed SWD data using a pilot from a GPS-synchronized top-drive sensor (Bakulin et al., 2020a). In contrast, this study utilizes a downhole pilot recording drill-bit noise signature for deconvolution and processing.

## SWD processing

SWD processing has primarily followed the sequence described by Bakulin et al. (2020a). However, it has two crucial distinctions, as outlined in Figure 2c. The key difference from the previous work is utilizing in processing the pilot signal from the memory-based downhole tool instead of the top-drive sensor. While the earlier work aimed to assess the system's real-time capabilities, this study focuses on more accurate but non-real-time capabilities with a pilot taken from the vertical component of the downhole sensor. Here, we seek to obtain the best quality data and maximize the utilization of the recorded SWD waveforms. While the near-bit pilot better captures a highly complex and random drill-bit source signature, it suffers from a substantial internal clock drift. Therefore, it cannot be used without an accurate time correction. Egorov et al. (2021) resolved this issue by applying a global optimization method to determine the delay time and linear drift between the downhole signal and the top-drive one. They also used a correlation-based method to estimate the residual nonlinear drift reaching millisecond alignment accuracy. Because both the top-drive sensor and surface data are GPS-synchronized, the data-driven alignment procedure delivers an alternative pilot useable for further processing. Then, it is correlated with surface data to collapse the random drill-bit signal to impulse-like arrival from a downhole point source. Finally, additional pilot deconvolution is applied to remove reverberations in the correlated data. The deconvolution operator is constructed in reverse time as a least-squares Wiener predictive filter with unit prediction distance (Poletto et al., 2001).

To enhance the S/N of the weak drill-bit signal, a vertical stacking operation is applied over a drill pipe's length, equivalent to 30 ft (approximately 9.1 m). Poletto and Miranda (2004) and Bakulin et al. (2020a) explained the details of the stacking operation

and its implications. For instance, autocorrelation of the stacked top-drive pilot over 30 ft drilling intervals has revealed strong signals traveling along the drillstring detectable down to about 6200 ft (Bakulin, 2020a). As a result, deconvolved common-bit gathers showed direct first-arriving waveforms. This study follows a similar processing flow but instead uses an aligned downhole pilot.

After vertical stacking, impulse-like common-source records with the shot position corresponding to the middle of the 30 ft stacked drilling interval are produced at every depth level. However, direct and reflected waves ignited by the drill-bit source are obscured by intense surface noise, as shown by Bakulin et al. (2020a). Such noise in a typical CSG is primarily caused by vibrating equipment of the drilling operation such as engines, shale shakers, and generators at the well site. This linear surface noise has a distinct characteristic of low dominant frequency compared to the signal ignited by the subsurface drill-bit source.

Another characteristic of the surface noise is that it is stationary. In contrast, the signal of the downhole drill-bit source changes as the bit penetrates deeper (Poletto and Miranda, 2004). Therefore, high-pass filtering is applied to the SWD data to suppress the unwanted surface noise and enhance the downhole drill-bit signal (Petronio et al., 1999; Wang et al., 2008). A 3D common-bit gather after high-pass filtering above 20 Hz is shown in Figure 2a. First arrivals are reasonably clear at some offsets/azimuths while becoming obscured at others. This happens because drill-bit seismic data were recorded using single-sensor geophones in a desert land environment with complex near-surface geology. In this region, land surface seismic data are acquired using nine to 72 geophones in the receiver array and two to five vibrators in the source array to deliver an acceptable prestack S/N (Bakulin et al., 2018). Previous studies with this particular SWD data set relied heavily on supergrouping (Bakulin et al., 2020a; Aldawood et al., 2021) to enhance the data and improve initially low S/N caused by the complex near-surface scattering.

In contrast to previous studies, we apply a more sophisticated enhancement technique of nonlinear beamforming (NLBF), fully using 3D acquisition geometry of SWD data (Bakulin et al., 2020b). Unlike supergrouping, NLBF does not assume knowledge of local event moveout. Instead, it performs a data-driven coherency search to find local moveouts. NLBF was applied in the receiver X-Y domain with a stacking aperture of 200 × 200 m. Figure 2b proves that NLBF significantly increases the S/N of the same common-bit gather in Figure 2a for all offsets and azimuths. Furthermore, enhancement enables robust 3D traveltime picking throughout the entire shallow section. Figure 2c summarizes all the processing steps showing the workflow that allowed effective processing of the recorded drill-bit seismic data with low S/N. In summary, source stacking (over the drill pipe length) and receiver beamforming are critical steps to improve the S/N of SWD single-sensor data from the desert environment. Coupled with the deconvolution using a high-fidelity downhole pilot, such processing led to the remarkable quality of 3D SWD data.

## Simple workflow for 1D velocity model building using 3D traveltimes from SWD data (190–1855 m)

First, let us build the most reliable 1D velocity for the entire section from shallow to deep (190–1855 m) using a simple workflow that leverages redundancy of 3D SWD data instead of picking a single receiver location as in previous studies. The simple workflow uses an approximation of vertical traveltime projection relying on straight-ray assumption. Because such an approximation is valid for small offsets, we only consider 3D SWD data with limited offsets of 180–500 m. The yellow circle in Figure 1a encloses blue and orange receivers used for shallow and deep drilling settings, respectively. While a small number of receivers with offsets smaller than 180 m were available (Figure 1b), they were strongly affected by rig-induced noise and hence were excluded from the inversion. Bakulin et al. (2020a) reconstructed a checkshot profile with the following limitations:

- The top-drive sensor pilot allowed the reconstruction only below 565 m depth. SWD data shallower than 565 m were too noisy to pick reliable first breaks.
- A single receiver with an offset of 475 m was selected because it provided the best quality data. However, most of the remaining data were unused.

Such an approach is typical for SWD applications, where real-time velocity updates are desired. However, it may be subjective as each geophysicist may select different receivers with the best quality data. Moreover, it may lead to a biased estimation due to variations of near-surface velocities. This study will address both limitations and provide a more reliable and extended 1D velocity profile, especially in the shallow subsurface.

Silvestrov et al. (2021) clearly showed that a downhole pilot leads to significant improvements in SWD data quality,

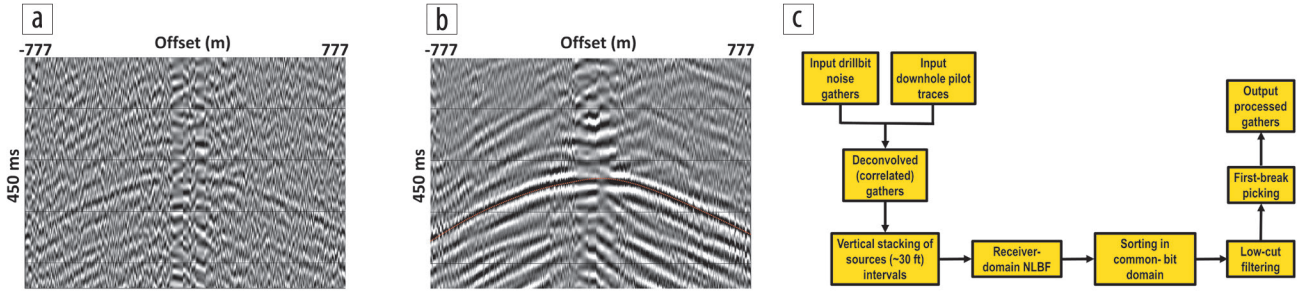


**Figure 2.** SWD data at various processing stages and the processing flow: (a) 3D common-bit gather at a depth of 766 m after deconvolution with the downhole pilot and low-cut filtering (20 Hz); (b) the same gather after additional application of NLBF; (c) full processing workflow. Three-dimensional gather is shown as a function of offset mapping westward and eastward half-planes into the negative and positive offsets, respectively (Figures 1a and 1b). The red curve marks first-break picks.

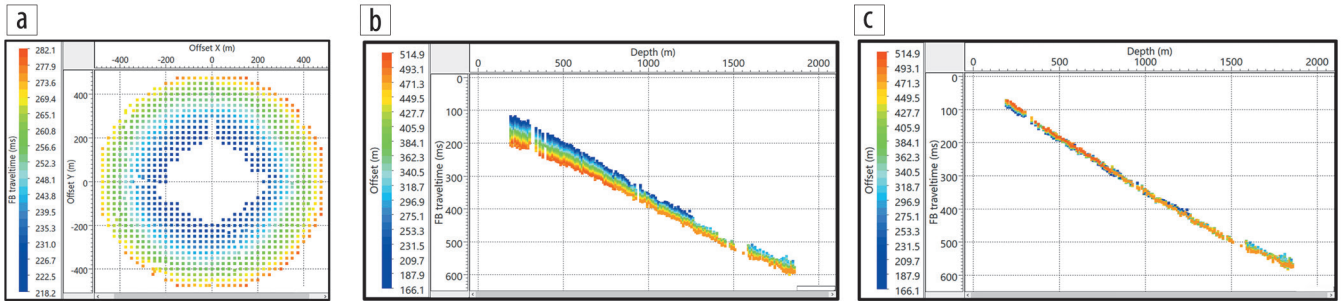


**Figure 3.** Checkshot profile reconstruction using simple workflow with the vertical projection of traveltimes: (a) first-break traveltimes map with offset ranges from 180 to 500 m from the well location; (b) picked traveltimes versus depth color-coded by offset; (c) traveltimes after vertical projection (assuming straight-ray assumption). A hole in the traveltime map (a) is caused by missing receivers on the drilling pad (Figure 1b). Observe noticeable offset dependency or spread of unprojected traveltimes on (b) as the longer offsets lead to larger first-break traveltimes. Vertical projection collapses the traveltimes into a tighter curve shown in (c).

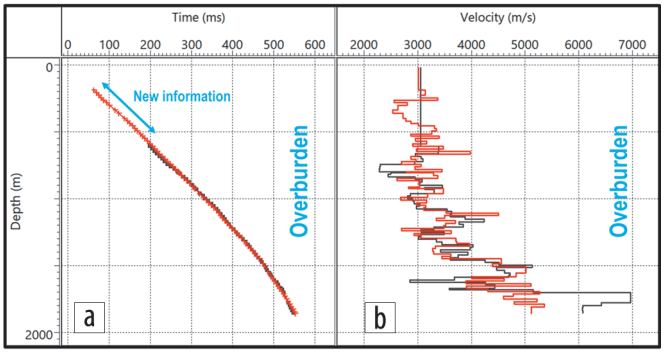


**Figure 4.** (a) Time-depth curves and (b) inverted velocity profiles using two different methods. Simple workflow with 3D traveltimes using a downhole pilot is shown in red. In contrast, the previous workflow with a single offset and top-drive pilot (Bakulin et al., 2020a) is in black. New workflow enables characterization of an additional 400 m of the shallow subsurface critical for seismic velocity model building and often missing from conventional wireline VSP.

particularly in shallow sections. Therefore, we utilize a downhole pilot instead of a top-drive one in this study. In addition, we shall use an entire set of 3D data instead. This section shows a simplified workflow using traveltime projection to zero offset to obtain a 1D velocity model for the entire section from 190 to 1855 m. Later, we apply a more advanced workflow that properly accounts for wave propagation along nonstraight rays and builds an alternative model for the shallow subsurface (0–800 m).

Data deconvolved with the downhole pilot and enhanced with NLBF allowed 3D traveltime picking from 190 to 1855 m depth. We stress that the downhole tool was run from 170 m depth onward. We only missed the shallowest interval (170–190 m), where data quality prevented us from reliable picking. Figure 3a shows a sampled first-break traveltimes map when bit depth is 589 m. The shallow setting of receivers (Figure 1b) is used here, whereas offsets are further restricted between 180 and 500 m. Figure 3b shows an overlay of time-depth curves from all offsets accumulating traveltime picks from approximately 1060 receiver locations. Color coding reveals a gradual increase of traveltime with offset. In this simple workflow, we project all traveltime picks to zero offset using commonly used straight-ray assumption and arrive at Figure 3c. Instead of picking a single "best" offset/azimuth with good-quality data, as in Bakulin et al. (2020a), we let all offsets and azimuths contribute so their votes would lead to the most statistically probable 1D velocity model. Vertical projection significantly reduces the traveltime offset dependency, validating that the velocity model may be close to 1D (Figure 3c).

We computed the mean value at each depth to develop the most likely average 1D velocity model. Then, to eliminate residual jittering, we smoothed and decimated the mean picks to 20 m, arriving at the average time-depth curve shown in Figure 4a by red crosses. Let us compare this curve with a previously obtained checkshot using a top-drive pilot. It was similarly obtained using vertical projection of traveltimes recorded at a single "best" offset/azimuth of 475 m followed by similar smoothing and decimation to 20 m depth interval (Figure 4a, black squares). Figure 4b displays corresponding 1D traveltime models inverted from two versions of the checkshot profile. Comparing two versions of the time-depth curves, we observe an overall reasonable agreement in the deeper part (Figure 4a) while still generating noticeable differences in the interval velocities (Figure 4b). Thus, results from the 3D workflow are expected to be more reliable due to averaging power of a much larger and redundant set of traveltimes. The most significant difference is in the shallow part, where a simple 3D workflow with downhole pilot allowed the characterization of an additional approximately 400 m of near surface (200–600 m) not attainable with the previous method. We believe such characterization is accurate and robust despite the lack of offsets below 180 m because of significant redundancy. Thus, invoking the downhole sensor, which provides the cleaner version of the drill-bit signature, and a 3D spread of geophones helped characterize the near-surface geology and build a more robust near-surface 1D compressional (P-wave) velocity model. The subsequent section compares this result with an advanced traveltime inversion to further support this point.

## 2D source focusing and imaging (190–1856 m)

Another way to use multichannel SWD data is to perform source focusing and imaging. It has been long established that drilling-induced sound intensity carries information about the mechanical properties of the drilled formation. The amplitude of top-drive or downhole sensor recordings was used to generate approximate pseudo-impedance logs using deterministic correlations (Lutz et al., 1972; Naville et al., 2004). However, deterministic relationships proved hard to find because of the complexity of the problem. The magnitude of vibration depends not only on formation properties but also on the drilling regime. Therefore,

it may become strongly distorted by drilling dysfunctions. Glubokovskikh et al. (2020) applied a machine learning algorithm to derive synthetic acoustic logs directly from near-bit vibrations recorded with the downhole tool. Similar information about source strength is encoded in the seismic amplitudes of SWD data.

Using field data, we demonstrate that as the drill bit penetrates through various layers, it produces a discernible seismic amplitude signature associated with the mechanical properties or seismic velocities of the layers. While the traveltime picks yield interval formation velocities (i.e., long-wavelength subsurface information), the amplitude signature obtained via source imaging/focusing provides high-resolution (high-wavenumber) information. Fink (2006) used time-reversal imaging to focus the recorded wavefield by the surface receivers at the subsurface source position using a reasonably accurate velocity model. Focusing first-arrival waveforms is more robust than localizing the source using traveltime methods, as the picks could be quite erroneous, especially for drill-bit seismic data characterized by low S/N. While focusing/imaging is possible using uncorrelated data, we perform an initial demonstration using correlated data in this study.

After deconvolving the recorded signal using the downhole pilot, the random drill-bit signature is collapsed to an impulsive point-scatterer downhole source. The kinematic behavior of the deconvolved wavefield, recorded on the surface, is described by a one-way traveltime path (Artman et al., 2010). Therefore, the focused source image of the drill bit $I(\mathbf{x})$ is mathematically obtained in the frequency domain by the following wavefield summation

$$I(\mathbf{x}) = \sum_{\omega} \sum_{A} d(A,\omega) e^{-i\omega(\tau_{\mathbf{x}A})}, \quad (1)$$

where $\mathbf{x}$ is the potential subsurface position of the drill-bit source, $\tau_{\mathbf{x}A}$ is the traveltime from such drill-bit position $\mathbf{x}$ to surface receiver $A$, and $d(A,\omega)$ is the recorded wavefield at the surface receiver station $A$ deconvolved using the downhole pilot trace. In essence, the recorded SWD signals are migrated in the simplest way by summing the data over the surface defined by the one-way traveltime from $\mathbf{x}$ to $A$. The final source image is obtained by applying a zero-lag imaging condition, computed by summing the migrated signals over all frequencies.

Applying the imaging equation of the source requires a smooth velocity model along the receiver line marked by the black arrow in Figure 1a. Therefore, we constructed a 2D velocity model from a smooth version of the checkshot profile, which was subsequently used to image the drill-bit source at all depth levels. To mitigate the migration artifacts, Aldawood et al. (2021) used a time gating around the first-arrival waveforms, limiting the source's emanating angle and the maximum dip at the source to 65° and 15°, respectively. Typical input gathers to the migration equation are shown in Figure 5a, where green curves show first-break picks.

Figure 5b shows a stacked migrated image of the drill-bit sources from all depth levels. The image clearly delineates the intervals at which the source was highly focused with strong amplitudes and intervals where some defocusing occurs, such as drilling through soft sediments, characterized by weak amplitudes. In addition, the image of drill-bit sources correlates with a compressional velocity log (Figure 5b, orange curve) obtained from

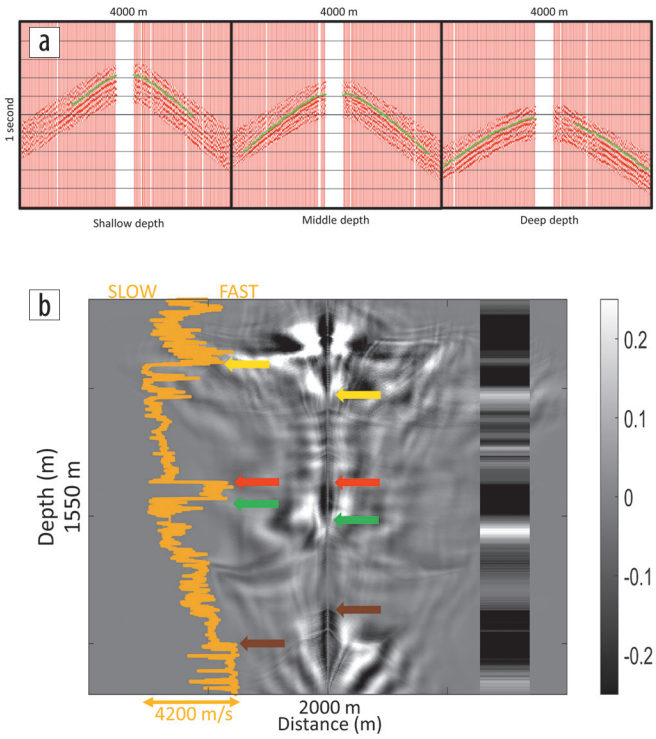


**Figure 5.** Two dimensional focusing and imaging of the drill-bit source: (a) typical common-bit gathers after time gating used for focusing exercise along with the first-break picks in green; (b) migrated and summed image of all the drill-bit sources at all depth levels after focusing overlaid by the compressional velocity log from a nearby well. The arrows denote key horizons associated with lithologic changes. Insert on the right side shows the intensity of the image extracted from the central location at the well.

an offset well 30 km away. Both wells sample the same subsurface layers, although their thicknesses vary laterally as identified by changing distance between major markers (arrows) on the drill-bit image from the current well and sonic log from an offset well.

Initially, the drilling was mainly through compacted carbonates manifested by the strongly focused sources from the surface. The yellow arrow marks a major lithologic change from compacted carbonates to a clastic rock formation consisting of interbedded shale and sand layers. The effect of this interbedding can be noted in the migrated image by multiple weak-to-strong amplitude anomalies. A highly compacted sandstone formation bounded between the red and green arrows has a distinct drill-bit signature manifested as a strong amplitude anomaly on the image. Such signature is well correlated with a high compressional velocity. Delineating the top and bottom of this layer is crucial, as drilling through such transitions requires careful optimization of drilling parameters, mainly mud weights, since loss circulations are often encountered near this zone. In addition, the section between the green and brown arrows is mainly composed of soft calcarenitic limestone, characterized by a fast rate of penetration and increased occurrence of drilling breaks. These formations exhibit weak amplitudes and less focused source images. Below the brown arrow, strong focused amplitudes reappear again, identifying entry into highly-compacted anhydrite formation. Note that all these geologic formations are present and marked by the arrows on the offset well sonic log, albeit with different thicknesses of layers.

DOI:10.1190/tle41050304.1

## Advanced workflow for 1D velocity model building using 3D traveltimes from SWD data (190–800 m)

While a simple workflow with geometric traveltime projection is popular, reliance on the straight-ray assumption in the presence of many highly contrasting layers may lead to less accurate results. This section applies a more advanced workflow to build a 1D velocity model from 3D SWD data. We restrict our focus to shallow drilling settings (0–800 m) with consistent geometry shown in Figure 1b. The shallow drilling setting ends at approximately 800 m, whereas the downhole tool was available from 170 m. Therefore, we have around 63 depth levels for SWD data sampled with a 30 ft (9.1 m) interval. A square geophone patch of 1100 × 1100 m has about 1900 sensors centered around the vertical well (Figure 1b). The offset/depth ratio of SWD data may exceed one and therefore contains a wide range of angles, enabling accurate characterization of the near-surface model, potentially including anisotropy.

Using a 3D SWD data set, we picked more than 100,000 first-break traveltimes. In contrast to a simple workflow with vertical projection, the advanced workflow utilizes 3D least-squares inversion of first-arrival traveltime fields based on ray tracing. The classical VSP-type inversion is obtained by solving the following linearized system of equations:

$$\mathbf{L}\Delta\mathbf{s} = \Delta\mathbf{t}, \tag{2}$$

where $\mathbf{L}$ is the forward modeling operator based on 3D two-point ray tracing. $\Delta\mathbf{s}$ is the vector of model parameters (slowness) updates, and $\Delta\mathbf{t}$ is the vector of all traveltime differences that the inversion process minimizes. We assume a laterally invariant velocity model to make the inversion robust and comparable with previous results. The least-squares solution $\Delta\mathbf{s}_{\mathbf{lsqr}}$ can be obtained as follows:

$$\Delta\mathbf{s}_{\mathrm{lsqr}} = (\mathbf{L}^{\mathrm{T}}\mathbf{L} + \alpha\mathbf{I})^{-1}\mathbf{L}^{\mathrm{T}}\Delta\mathbf{t}, \tag{3}$$

where $\alpha$ is a small scalar used to stabilize the ill-posed system of equations. The solution is obtained iteratively until the norm of the model parameter update vector is smaller than a specified threshold.

An initial velocity model with a constant velocity of 3000 m/s was selected based on the reconstructed checkshot from the simple workflow, which applies a projection technique under a straight-ray assumption (Figure 4b). A 3D traveltime inversion with 32 layers leads to the model shown in Figure 6. Despite starting from a constant velocity model, inversion recovers high- and low-velocity layers with significant contrast. Figure 6b shows a 2D slice through the inverted 1D model and ray trajectories connecting fixed receiver at the surface to all downhole source positions.

Figure 7 shows selected 3D common-bit gathers for several depth levels along with the progression of traveltime picks. The initial model leads to predicted traveltime curves shown in red that do not match the observed picks in blue. In contrast, orange picks from the inverted model provide a good overall description of the experimental traveltimes. Blue picks exhibit nonhyperbolic behavior caused by small-scale velocity changes in the near surface, statics, and data quality variation. We intentionally ignore those details and instead seek a good average and hyperbolic description that constrains the most likely 1D velocity model.

Figure 8 compares near-surface velocities inverted using the simple method with vertical projections and the advanced workflow with 3D traveltime tomography. Both profiles exhibit a high degree of similarity and reveal near-surface velocities at high resolution. In addition, major markers and velocity inversions are also in agreement between the two models. However, there are discrepancies in the shallowest 200 m of the near-surface model. The 3D inversion of picks from all offsets is expected to be more accurate. It yields a profile closer to the truth with a slower average velocity in the shallowest section. For the shallowest drill-bit source position of 200 m, the minimum offset of 180 m (Figure 3a) implies that the angles used are above

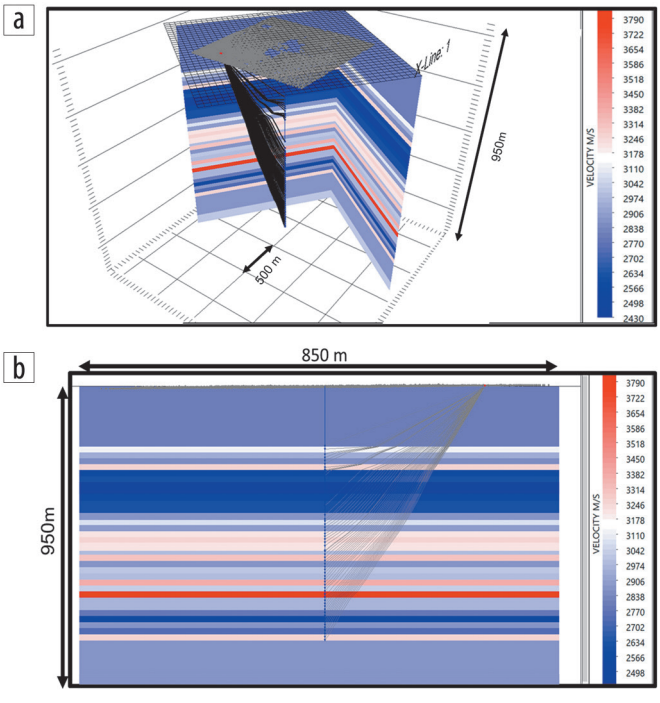


**Figure 6.** Three-dimensional traveltime tomography inversion for 1D velocity model: (a) a 3D view of the acquisition geometry and inverted P-wave velocity model; (b) 2D slice of the inverted velocity model. The initial model with a constant velocity of 3000 m/s was used. Both figures show ray trajectories from a specific surface receiver to drill-bit sources at different depth levels.

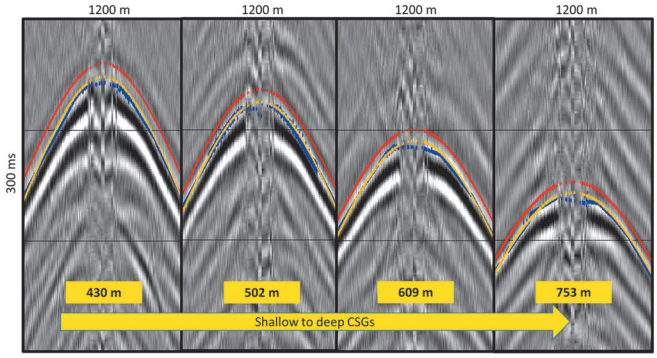


**Figure 7.** Typical common-bit gathers at different depth levels. Different colors denote various traveltimes: blue = picked first-break times, red = traveltimes computed using the initial model, and orange = predicted times using the final inverted 1D model.

DOI:10.1190/tle41050304.1

approximately 40°. For such large angles of incidence, the vertical projection method is not expected to be accurate. If the actual model above 200 m would be homogenous, then simple and advanced workflows should agree. However, seismic uphole data (Figure 9) from the area suggest that the shallow near surface (0–50 m) exhibits a strong vertical gradient. Significant velocity variation is also present between 100 and 200 m, as suggested by the sonic log from an offset well (Figure 8b). In the case of strong vertical heterogeneity and large angles of incidence, the average descriptions using 3D traveltime tomography and simplistic vertical projection are expected to differ. Indeed, the advanced workflow gives 7% slower velocity in the first 200 m than the simple one, suggesting that a crude description of shallow near surface by a single homogeneous layer is not plausible. In addition, a slower velocity value is closer to the average velocity expected when combining uphole data (0–50 m) from Figure 9 and sonic log segment (100–200 m) from Figure 8b. Suppose a downhole sensor would be run in the first drilling section (0–170 m). In that case, we might have a chance to characterize velocity variation within the shallow near surface. Another alternative is to acquire an uphole seismic survey next to the deep well of interest.

At last, let us crosscheck the inverted model against the compressional velocity log from an offset well (Figure 8b). Again, the two profiles resemble each other, and key near-surface horizons can be marked on both the sonic and inverted profiles, validating the robustness of the inversion process.

Finally, let us demonstrate a clear correspondence between kinematic signatures (traveltimes and velocities) and dynamic SWD signatures (amplitudes) from source focusing. Figure 10a shows that going from a hard layer to a soft one, the SWD amplitude switches from strong to weak or nearly undetectable. Likewise, going from a soft to hard layer, we observe the low amplitude turning into a strong one. Across the interface marked by the brown arrow, the velocity changes from fast to relatively slow values consistent with a highly fractured zone. This agrees with the amplitude signature of the first-arrival waveforms changing from strong amplitudes with high S/N to a weak amplitude with low S/N. Likewise, as the drill bit exits this fractured zone (the black arrow), the amplitude on the SWD gathers becomes strong, again exhibiting higher S/N. The low-velocity zone between the brown and black arrows is known for the increased chance of circulation loss while drilling associated with a known near-surface unconformity. Reilly et al. (2010) mentioned the abundance of similar shallow anomalies with significant karstifications and channeling and illustrated their defocusing effects on 3D seismic images. Figure 10b shows a surface outcrop with a similar heavily karstified layer in the near surface.

Another interface, marked by the yellow arrow, indicates the transition from a relatively faster layer to a slower one. This interface is another known unconformity transiting from highly compacted carbonates to a softer streak of shale layers. Therefore, the amplitude signature clearly changes from strong in carbonates to weak in shale. Stronger drill-bit sources while crushing hard layers exhibit higher S/N with an easily trackable event. In contrast, weaker sources while drilling soft layers exhibit low S/N with events that are harder to track or even completely drowned in the background noise. The last crucial near-surface unconformity, denoted by the green arrow, marks the drilling through a highly compacted thick layer of shale with a relatively higher velocity than the overlaying softer carbonate sediments.

## Conclusions

We present a comprehensive case study applying 3D SWD data on an onshore field to reconstruct a robust 1D velocity model, obtain a 2D image of source focusing, and build a high-resolution near-surface velocity model using 3D inversion of first-break offset traveltimes. The downhole pilot from a near-bit tool is utilized for deconvolution to reconstruct impulse-like signals from the drill-bit noise recorded by surface receivers. A specialized workflow including vertical stacking of sources, data enhancement using NLBF, and low-cut filtering generates reliable 3D SWD offset gathers with improved S/N. Utilizing the downhole pilot and the large ensemble of picks from the carpet of receivers significantly

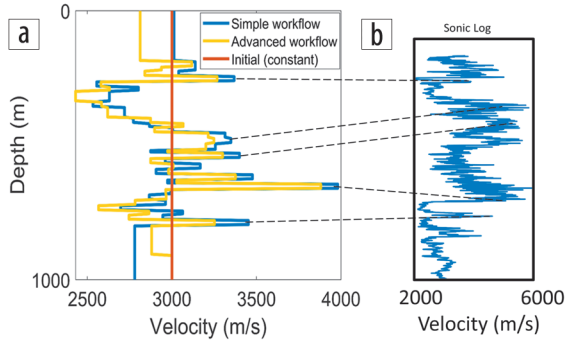


**Figure 8.** Interval velocity profiles obtained using different methods: (a) comparison of inverted velocities using simple (blue) and advanced (yellow) workflows with the initial model shown in red; (b) compressional velocity log from an offset well. Simple and advanced workflows deliver similar velocity profiles. In addition, the sonic log from offset wells helps validate the inverted profile. Major near-surface horizons, denoted by the dashed black lines, show good agreement between the log and inverted interval velocities from SWD data.

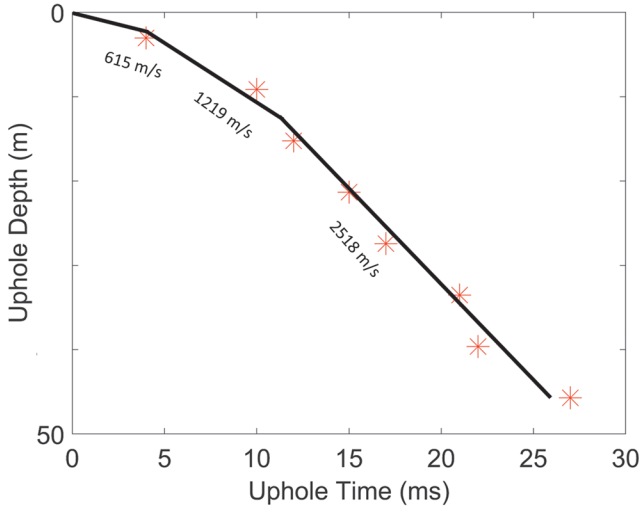


**Figure 9.** Time-depth curve obtained from an uphole survey in the same area as a deep well of interest. Substantial vertical velocity variation is observed primarily in shallow layers.

improves the reconstructed checkshot profile. It also extends the reverse VSP to as shallow as 190 m.

We also utilize an advanced workflow to build a high-resolution 1D velocity model for shallow subsurface down to 800 m using 3D SWD data. The large ensemble of traveltimes is simultaneously inverted using 3D traveltime tomography to produce a high-resolution 1D velocity model identifying karstified layers.

We identify how the relative amplitude information extracted from SWD could be used for a more resolved characterization than kinematic information. A 2D focusing of the sources along an east-west striking line produces a migrated image of the drill-bit source at all depth levels. The focused images show a discernible seismic amplitude signature associated with major lithologic changes. In addition, such signatures seem to contain high-resolution information comparable to what is seen in wireline acoustic logs.

This case study validates the capability of the SWD data with a downhole pilot to characterize shallow subsurface in a desert environment. Reliable velocity profiles are obtained from shallow (about 190 m) to deep (about 1855 m) depths. Both kinematic and dynamic signatures of SWD data help localize and identify key markers associated with drilling hazards. A downhole pilot is a fundamental enabler to various techniques that better characterize the shallow and deeper subsurface. TLE

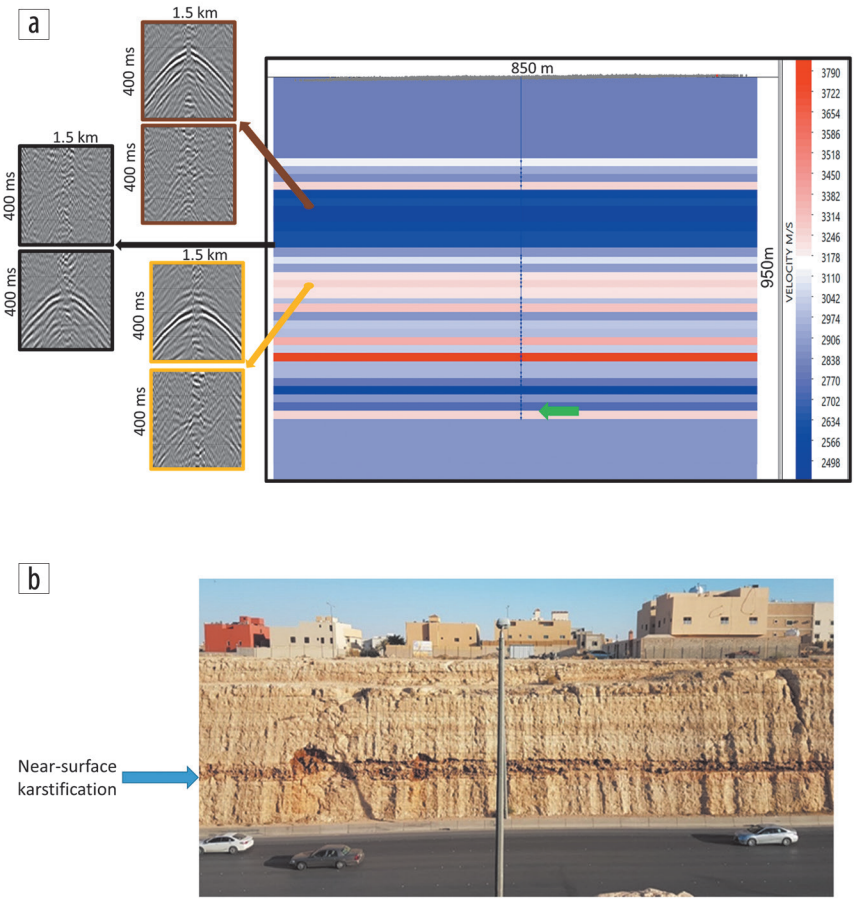


**Figure 10.** Correspondence between kinematic signatures (traveltimes and velocities) and dynamic SWD signatures (amplitudes): (a) 2D cross section of inverted velocity model along with selected SWD gathers recorded above and below major velocity contrasts; (b) an outcrop photo with heavily karstified layer analogous to the low-velocity zone between the brown and black arrows in (a). The arrows mark major impedance contrasts. The associated gathers show how the dynamic seismic signatures (amplitude strength and S/N) change across the interfaces. Photo courtesy of Ahmad Ramdani (KAUST).

## Acknowledgments

We thank Emad Hemyari (formerly Saudi Aramco) for support in data processing and analysis. In addition, we are grateful to Flavio Poletto (OGS) for productive discussions and technical advice.

## Data and materials availability

Data associated with this research are confidential and cannot be released.

Corresponding author: ali.dawood.18@aramco.com

## References

Aldawood, A., E. Hemyari, I. Silvestrov, and A. Bakulin, 2021, Imaging ahead of and around the bit in a desert environment: DrillCAM field trial with wireless geophones and top-drive sensor: The Leading Edge, **40**, no. 5, 374–381, https://doi.org/10.1190/tle40050374.1.

Al-Muhaidib, A. M., Y. Liu, P. Golikov, E. Al-Hemyari, Y. Luo, and M. N. Al-Ali, 2018, DrillCam: A fully integrated real-time system to image and predict ahead and around the bit: 88th Annual International Meeting, SEG, Expanded Abstracts, 719–723, https://doi.org/10.1190/segam2018-2995323.1.

Artman, B., I. Podladtchikov, and B. Witten, 2010, Source location using time-reverse imaging: Geophysical Prospecting, **58**, no. 5, 861–873, https://doi.org/10.1111/j.1365-2478.2010.00911.x.

Bakulin, A., A. Aldawood, I. Silvestrov, E. Hemyari, and F. Poletto, 2020a, Seismic-while-drilling applications from the first DrillCAM trial with wireless geophones and instrumented top drive: The Leading Edge, **39**, no. 6, 422–429, https://doi.org/10.1190/tle39060422.1.

Bakulin, A., P. Golikov, M. Dmitriev, D. Neklyudov, P. Leger, and V. Dolgov, 2018, Application of supergrouping to enhance 3D prestack seismic data from a desert environment: The Leading Edge, **37**, no. 3, 200–207, https://doi.org/10.1190/tle37030200.1.

Bakulin, A., P. Golikov, R. Smith, K. Erickson, I. Silvestrov, and M. Al-Ali, 2017, Smart DAS upholes for simultaneous land near-surface characterization and subsurface imaging: The Leading Edge, **36**, no. 12, 1001–1008, https://doi.org/10.1190/tle36121001.1.

Bakulin, A., E. Hemyari, and I. Silvestrov, 2019, Acquisition trial of DrillCAM: Real-time seismic with wireless geophones, instrumented top drive and near-bit accelerometer: 89th Annual International Meeting, SEG, Expanded Abstracts, 157–160, https://doi.org/10.1190/segam2019-3214516.1.

Bakulin, A., and I. Silvestrov, 2021, Understanding acquisition and processing challenges in the desert environment through SEAM

Arid and Barrett models: First International Meeting for Applied Geoscience and Energy, SEG/AAPG, Expanded Abstracts, 2824–2829, https://doi.org/10.1190/segam2021-3583002.1.

Bakulin, A., I. Silvestrov, M. Dmitriev, D. Neklyudov, M. Protasov, K. Gadylshin, and V. Dolgov, 2020b, Nonlinear beamforming for enhancement of 3D prestack land seismic data: Geophysics, **85**, no. 3, V283–V296, https://doi.org/10.1190/geo2019-0341.1.

Bertelli, L., and F. di Cesare, 1999, Improving the subsurface geological model while drilling: First Break, **17**, no. 6, 223–228, https://doi.org/10.1046/j.1365-2397.1999.00706.x.

Egorov, A., I. Silvestrov, A. Bakulin, and P. Golikov, 2021, Research note: Automated data-driven alignment of near-bit and top-drive vibration sensors for seismic while drilling and beyond: Geophysical Prospecting, **69**, no. 7, 1560–1568, https://doi.org/10.1111/1365-2478.13119.

Fink, M., 2006, Time-reversal acoustics in complex environments: Geophysics, **71**, no. 4, SI151–SI164, https://doi.org/10.1190/1.2215356.

Glubokovskikh, S., A. Bakulin, R. Smith, and I. Silvestrov, 2020, Machine learning algorithms for real-time prediction of the sonic logs based on drilling parameters and downhole accelerometers: 90th Annual International Meeting, SEG, Expanded Abstracts, 405–409, https://doi.org/10.1190/segam2020-3427085.1.

Greenberg, J., 2008, Seismic while drilling keeps bit turning to right while acquiring key real-time data: Drilling Contractor, **64**, no. 2, 44–45.

Haldorsen, J. B. U., D. E. Miller, and J. J. Walsh, 1995, Walk-away VSP using drill noise as a source: Geophysics, **60**, no. 4, 978–997, https://doi.org/10.1190/1.1443863.

Hardage, B. A., 2000, Vertical seismic profiling: Principles: Pergamon Press.

Khaled O. S., A. M. Al-Ateeqi A. R. James, and R. J. Meehan, 1996, Seismic-while-drilling in Kuwait results and applications: GeoArabia, **1**, no. 4, 531–550, https://doi.org/10.2113/geoarabia0104531.

Lutz, J., M. Raynaud, S. Gestalder, C. Quichaud, J. Raynal, and J. A. Muckerloy, 1972, Instantaneous logging based on a dynamic theory of drilling: Journal of Petroleum Technology, **24**, no. 6, 750–758, https://doi.org/10.2118/3604-PA.

Miranda, F., L. Aleotti, F. Abramo, F. Poletto, A. Craglietto, S. Persoglia, and F. Rocca, 1996, Impact of the seismic 'while drilling' technique on exploration wells: First Break, **14**, no. 2, https://doi.org/10.3997/1365-2397.1996004.

Naville, C., S. Serbutoviez, A. Throo, O. Vincké, and F. Cecconi, 2004, Seismic while drilling (SWD) techniques with downhole measurements, introduced by IFP and its partners in 1990–2000: Oil & Gas Science and Technology, **59**, no. 4, 371–403, https://doi.org/10.2516/ogst:2004027.

Poletto, F., M. Malusa, and F. Miranda, 2001, Numerical modeling and interpretation of drillstring waves: Geophysics, **66**, no. 5, 1569–1581, https://doi.org/10.1190/1.1487102.

Poletto, F., and F. Miranda, 2004, Seismic while drilling: Fundamentals of drill-bit seismic for exploration: Elsevier.

Poletto, F., L. Petronio, F. Miranda, M. Malusa, A. Schleifer, P. Corubolo, C. Bellezza, R. Miandro, and B. Gressetvold, 2003, Prediction and 3D imaging while drilling by drill-bit 3D RVSP: 65th Conference and Exhibition, EAGE, Extended Abstracts, https://doi.org/10.3997/2214-4609-pdb.6.P221.

Petronio, L., F. Poletto, F. Miranda, and G. Dordolo, 1999, Optimization of receiver pattern in seismic-while-drilling: 69th Annual International Meeting, SEG, Expanded Abstracts, 164–167, https://doi.org/10.1190/1.1820847.

Rector, J. W., and B. P. Marion, 1991, The use of drill-bit energy as a downhole seismic source: Geophysics, **56**, no. 5, 628–634, https://doi.org/10.1190/1.1443079.

Reilly, J. M., A. P. Shatilo, and Z. J. Shevchek, 2010, The case for separate sensor processing: Meeting the imaging challenge in a producing carbonate field in the Middle East: The Leading Edge, **29**, no. 10, 1240–1249, https://doi.org/10.1190/1.3496914.

Rocca, F., M. Vassallo, and G. Bernasconi, 2005, Three-dimensional seismic-while-drilling (SWD) migration in the angular frequency domain: Geophysics, **70**, no. 6, S111–S120, https://doi.org/10.1190/1.2106050.

Silvestrov, I., A. Bakulin, E. Hemyari, A. Aldawood, and A. Egorov, 2021, Seismic-while-drilling with a pilot signal from a downhole memory-based vibration sensor: First International Meeting for Applied Geoscience and Energy, SEG/AAPG, Expanded Abstracts, 3058–3062, https://doi.org/10.1190/segam2021-3582705.1.

Wang, L., H. Liu, S. Tong, and M. Wei, 2008, Extracting the weak signal of the drill-bit from seismic while drilling data: International Workshop on Education Technology and Training and International Workshop on Geoscience and Remote Sensing, IEEE, 604–608, https://doi.org/10.1109/ETTandGRS.2008.86.

Zhou, B., I. Mason, S. Greenhalgh, and S. Subramaniyan, 2015, Seeing coal-seam top ahead of the drill bit through seismic-while-drilling: Geophysical Prospecting, **63**, no. 1, 166–182, https://doi.org/10.1111/1365-2478.12172.